# Robust and Low Complexity Bayesian Data Fusion for Hybrid Cooperative Vehicular Localization

G.M. Hoang[†‡], B. Denis[†], J. Härri[‡], D. T.M. Slock[‡]
[†]CEA-Leti, MINATEC Campus, 17 avenue des Martyrs, 38054 Grenoble, France
[‡]EURECOM, SophiaTech Campus, 450 route des Chappes, 06904 Biot, France
E-mails:{giaminh.hoang, benoit.denis}@cea.fr, {jerome.haerri, dirk.slock}@eurecom.fr

***Abstract*—This paper addresses Particle Filter (PF)-based hybrid Cooperative Localization (CLoc) strategies consisting of fusing *absolute* position information from embedded Global Navigation Satellite System (GNSS) with *relative* distance-dependent estimates using Impulse Radio - Ultra WideBand (IR-UWB) technology. Such hybrid GNSS/IR-UWB CLoc yet cannot benefit from the high precision estimates from the IR-UWB due to the disparity between GNSS position and IR-UWB V2V range measurement noises, leading to a divergence in CLoc accuracy. This paper first investigates the source of such counter-intuitive effect, and second proposes a novel adaptive Bayesian dithering technique to improve the efficiency of GNSS/IR-UWB fusion-based CLoc. This strategy increases the probability to reach a 20 cm accuracy from 50% (conventional IR-UWB and WiFi PF) to 95%.**

## I. Introduction

Cooperative Localization (CLoc) relying on radio-based ranging is a promising complementary strategy to improve Global Navigation Satellite System (GNSS) positioning accuracy required by future Cooperative Intelligent Transport System (C-ITS) applications [1]–[6]. In this context, an "ego" vehicle considers its neighbors as potential "virtual anchors" [2], [3], [5], [7] (i.e. mobile anchors with only approximate knowledge about their own positions). The general principle of vehicular CLoc works in three phases. First, each vehicle piggybacks its *absolute* position information in a "Beacon" sent over "V2X" communication links[1]. Through the reception of these "Beacons", a given "ego" vehicle becomes aware of the *absolute* position estimates of its neighbors. The second phase consists of using the "Beacon" signal statistics to sample *relative* position-dependent information from these "virtual anchors" (e.g., Vehicle-to-Vehicle (V2V) distances, relative angles...). Ad hoc trilateration can then be locally applied to fuse the latter information with on-board GNSS position estimates and further enhance the *absolute* localization (See Fig. 1). In the final phase, the "ego" vehicle cooperates to improve the localization of other vehicles by further broadcasting its fusion results in subsequent "Beacons".

CLoc has already been applied in [1], [3], [6] to fuse on-board GNSS positions with opportunistic V2V Received Signal Strength Indicators (RSSIs) out of "Beacons" called Cooperative Awareness Messages (CAMs) [8], relying on the V2X ITS-G5 technology[2]. A major advantage of using V2V RSSI lies in the full compliance with future ITS-G5 connected vehicles[3]. Yet, V2V RSSI-based ranging is a highly parametric technique that requires model calibration. It offers limited accuracy and reliability, especially in non-static multipath environments, where channel parameters (i.e., path loss, shadowing, etc.) may fluctuate significantly depending on the operating environment [1], [2]. Thus, it has been proposed in [5] to replace ITS-G5-based RSSI readings by Impulse Radio - Ultra WideBand (IR-UWB) Time-of-Flight (ToF) measurements. Compared to ITS-G5, the latter technology is indeed known to provide centimeter-level distance resolutions. This approach thus combines local on-board GNSS positions, neighboring fusion-based estimated positions (still broadcast over V2V communication links using the ITS-G5 communication technology), and IR-UWB ToF-based range measurements in a classical Particle Filter (PF) estimation framework. However, divergence in the CLoc accuracy resulting from unbalanced levels of uncertainty between GNSS and IR-UWB have also been pointed out in [5], requiring a 2-step scheduling method mostly applicable in restrictive heterogeneous scenarios where high-class GNSS devices must be available at least at some vehicles.

Considering less restrictive scenarios, we investigate in this paper the source of the counter-intuitive divergence in vehicular hybrid GNSS/IR-UWB CLoc, and make the following two main contributions: (i) we illustrate the impact and cost of fusing information sources with significantly different levels of uncertainty (e.g., GNSS and IR-UWB ToF); (ii) we propose an adaptive Bayesian dithering technique, where dither noise is gradually added from a predicted theoretical lower bound until the divergence is fully mitigated. We compare our proposal over four different other strategies, namely pure GNSS, GNSS+RSSI CLoc, GNSS+IR-UWB CLoc and even Extended Kalman Filter (EKF) CLoc.

The paper is organized as follows. Section II introduces concepts behind hybrid CLoc, while Section III presents the main contributions of this paper. Simulation results and benchmarking are provided in Section IV. Finally, Section V concludes the paper and provides an outlook on future works.

[1]To remain technology neutral, a "Beacon" is a message periodically broadcast by each node, while "V2X" (Vehicle-to-X) refers to any technology capable of Device-to-Device (D2D) communication in a vehicular context.

[2]CAM and ITS-G5 are European counterparts to the Basic Safety Message (BSM) and Dedicated Short Range Communication (DSRC) in the US.

[3]ITS-G5 is expected to be available in every vehicle sold from 2019.

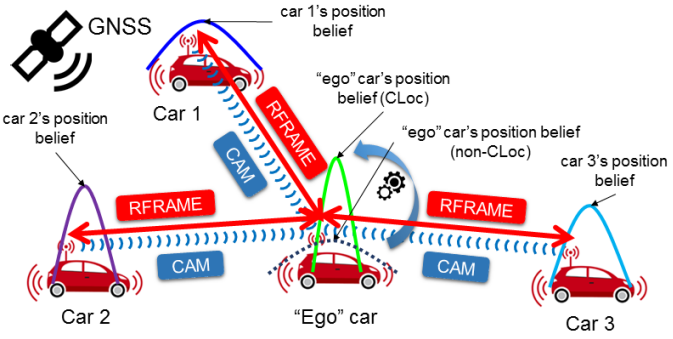


Fig. 1. "Ego" car receiving CAMs and exchanging ranging frames RFRAME from/with single-hop "virtual anchors" to perform distributed CLoc. The CLoc position beliefs (i.e., after fusing GNSS with ITS-G5 RSSIs or IR-UWB ranges) are expected to be more concentrated than that of non-CLoc (i.e., with standalone GNSS only).

## II. Problem Formulation

### A. Cooperative Localization in VANETs

We consider a set of connected GNSS-equipped vehicles exchanging CAMs over ITS-G5 channels. These vehicles are also endowed with IR-UWB ranging capabilities. The goal of an "ego" vehicle is to infer its position (as part of its so-called "state" in the following) based on its own estimated GNSS position, on V2V IR-UWB ranges with respect to single-hop neighbors, and on imperfect state information from these neighbors, considered as "virtual anchors" (i.e., estimated locations and their related uncertainties, encapsulated in the CAMs). Fig. 1 illustrates the CLoc concept. We do not consider V2I communications here to assist positioning, though Road Side Units (RSUs) could be helpful. Our aim is to remain independent from any additional infrastructure (i.e., other than the GNSS infrastructure itself), which not only significantly reduces deployment costs but also operates seamlessly on any road.

### B. System Model

We consider a VANET consisting of a set $\mathcal{V}$ of connected vehicles. At each vehicle $i \in \mathcal{V}$, time is locally sampled by $t_{i,0}, t_{i,1}, \ldots, t_{i,k}$ which are simply denoted by the discrete time index $k$[4]. Vehicles' states are denoted by $\boldsymbol{\theta}_{i,k} = (\mathbf{x}_{i,k}^\dagger, \mathbf{y}_{i,k}^\dagger)^\dagger$, where $\mathbf{x}_{i,k} = (x_{i,k}, y_{i,k})^\dagger$, $\mathbf{v}_{i,k} = (v_{i,k}^x, v_{i,k}^y)^\dagger$ are 2-D absolute position and 2-D velocity respectively. In this paper, these states evolve according to a mobility model such as Gauss-Markov model suitable for vehicular context[5]

$$\boldsymbol{\theta}_{i,k+1} = \begin{pmatrix} \mathbf{I}_2 & \alpha\Delta T \cdot \mathbf{I}_2 \\ \mathbf{0}_2 & \alpha \cdot \mathbf{I}_2 \end{pmatrix} \boldsymbol{\theta}_{i,k} + (1-\alpha) \begin{pmatrix} \Delta T \cdot \mathbf{I}_2 \\ \mathbf{I}_2 \end{pmatrix} \bar{\mathbf{v}}_i + \sqrt{1-\alpha^2} \begin{pmatrix} \Delta T^2 \cdot \mathbf{I}_2 \\ \Delta T \cdot \mathbf{I}_2 \end{pmatrix} \mathbf{w}_{i,k}, \quad (1)$$

[4]Due to asynchronously sampled time instants, the index $k$ is locally meaningful. For notation brevity, the subscript indicating the vehicle index is dropped. If, however, it is included, the associated variable is strictly considered w.r.t. the timeline of the stated vehicle index.

[5]We assume that each vehicle has knowledge about its own and neighboring mobility models (by including this information in the CAMs). These mobility statistics are then used to perform prediction of both "ego" and neighbors' estimated locations and resynchronize related data before fusion [2], [3].

where $\alpha$ is the memory level, $\Delta T$ the time step, $\bar{\mathbf{v}}_i = (\bar{v}_i^x, \bar{v}_i^y)^\dagger$ the asymptotic 2-D velocity, $\mathbf{w}_{i,k} = (w_{i,k}^x, w_{i,k}^y)^\dagger$ the 2-D process Gaussian noise, $\mathbf{I}_2$ the identity matrix of size $2 \times 2$.

At discrete time $t_{i,k}$, the "ego" vehicle $i$ has the set $\mathcal{S}_{\to i,k}$ of "virtual anchors" and acquires up to three different types of measurements, which are interdependently produced by a GNSS receiver, an IR-UWB transceiver or ITS-G5 on-board unit respectively.

*1) GNSS Absolute Position:* The 2-D estimated position from GNSS $\mathbf{p}_{i,k} = (p_{i,k}^x, p_{i,k}^y)^\dagger$ is affected by an additive noise term $\mathbf{n}_{i,k} = (n_{i,k}^x, n_{i,k}^y)^\dagger \sim \mathcal{N}((0,0)^\dagger, \sigma_{\text{GNSS}}^2 \mathbf{I}_2)$ [3], [6], [7], $\sigma_{\text{GNSS}}$ is the GNSS noise standard deviation

$$p_{i,k}^x = x_{i,k} + n_{i,k}^x, \quad p_{i,k}^y = y_{i,k} + n_{i,k}^y. \quad (2)$$

*2) IR-UWB V2V Ranges:* Through a cooperative ranging protocol (e.g., based on the ToF estimation of transmitted packets involved in multiple-way handshake transactions [9]), vehicle $i$ at time $t_{i,k}$ estimates the V2V distance $z_{j\to i,k}$ to node $j$, $j \in \mathcal{S}_{\to i,k}$ in position $\mathbf{x}_{j,k_i}$

$$z_{j\to i,k} = \|\mathbf{x}_{i,k} - \mathbf{x}_{j,k_i}\| + n_{j\to i,k}, \quad (3)$$

where ranging noise $n_{j\to i,k} \sim \mathcal{N}(0, \sigma_{\text{UWB}}^2)$ and $\sigma_{\text{UWB}}$ is the ranging noise standard deviation.

*3) V2V Received Power:* Out of a received CAM, the RSSI $z_{j\to i,k}$ (on a dB scale) measured by vehicle $i$ at time $t_{i,k}$ with respect to vehicle $j$, $j \in \mathcal{S}_{\to i,k}$ in position $\mathbf{x}_{j,k_i}$ is assumed to follow the widely used log-distance path loss model [10]

$$z_{j\to i,k} = P(d_0) - 10 n_p \log_{10}(\|\mathbf{x}_{i,k} - \mathbf{x}_{j,k_i}\|) + X_{j\to i,k}, \quad (4)$$

where $P(d_0)$ [dBm] is the average received power at a reference distance $d_0$, $n_p$ the path loss exponent, $X_{j\to i,k} \sim \mathcal{N}(0, \sigma_{\text{Sh}}^2)$, and $\sigma_{\text{Sh}}$ the shadowing standard deviation.

The later range-dependent radio metric is introduced mostly for benchmark purposes with IR-UWB ToF-based ranges, in terms of their final PF-based fusion results. Finally, we introduce the following set notation to gather different vehicles' variables: stacked state of "virtual anchors" $\boldsymbol{\theta}_{\mathcal{S}\to i,k} = \{\boldsymbol{\theta}_{j,k_i} | \forall j \in \mathcal{S}_{\to i,k}\}$ and $\boldsymbol{\theta}_{\mathcal{S}\to i,k^-} = \{\boldsymbol{\theta}_{j,k<k_i} | \forall j \in \mathcal{S}_{\to i,k}\}$; full stacked state $\boldsymbol{\theta}_{i\cup\mathcal{S},k} = (\boldsymbol{\theta}_{i,k}^\dagger, \boldsymbol{\theta}_{\mathcal{S}\to i,k}^\dagger)^\dagger$; V2V measurement vector $\mathbf{z}_{\mathcal{S}\to i,k} = \{z_{j\to i,k} | \forall j \in \mathcal{S}_{\to i,k}\}$; and full measurement vector $\mathbf{z}_{i,k} = (\mathbf{p}_{i,k}^\dagger, \mathbf{z}_{\mathcal{S}\to i,k}^\dagger)^\dagger$.

### C. Bootstrap PF for VANETs

PF is attractive for nonlinear sequential state estimation when Kalman Filter (KF) based methods may diverge. Moreover, PF is intrinsically nonparametric w.r.t. the posterior density, which may be arbitrarily complex and multimodal. In PF, the posterior density $p(\boldsymbol{\theta}_{i,k} | \mathbf{z}_{i,1:k})$ is approximated by a particle cloud of $P$ random samples $\{\boldsymbol{\theta}_{i,k}^{(p)}\}_{p=1}^P$ and associated weights $\{w_{i,k}^{(p)}\}_{p=1}^P$ [11]–[13] i.e., $p(\boldsymbol{\theta}_{i,k} | \mathbf{z}_{1:k}) \approx \sum_{p=1}^P w_{i,k}^{(p)} \delta(\boldsymbol{\theta}_{i,k} - \boldsymbol{\theta}_{i,k}^{(p)})$, where $\delta(\cdot)$ is the Dirac delta function. However, it is challenging and expensive from the computation point of view to draw samples directly from $p(\boldsymbol{\theta}_{i,k} | \mathbf{z}_{i,1:k})$ due to its complex functional form [11]–[13].

**Algorithm 1** Bootstrap PF (iteration $k$, "ego" vehicle $i$)

1: **CAM Collection:** Receive CAMs from the set $\mathcal{N}_{\to i,k}$ of perceived neighbors, exact the parametric beliefs, and draw samples to reconstruct the approximated particle clouds $\{\tilde{\boldsymbol{\theta}}_{j,k}^{(p)}, 1/P\}_{p=1}^{P}$, $j \in \mathcal{N}_{\to i,k}$.

2: **Data Resynchronization:** Perform prediction of both "ego" and neighboring particle clouds based on mobility models at time $t_{i,k}$

$$\boldsymbol{\theta}_{i,k}^{(p)} \sim p(\boldsymbol{\theta}_{i,k}|\boldsymbol{\theta}_{i,k-1}^{(p)}), \qquad p = 1, \ldots, P,$$
$$\boldsymbol{\theta}_{j,k_i}^{(p)} \sim p(\boldsymbol{\theta}_{j,k_i}|\tilde{\boldsymbol{\theta}}_{j,k}^{(p)}), \qquad p = 1, \ldots, P, \quad j \in \mathcal{N}_{\to i,k}.$$

3: **Observation Update:** Select the subset $\mathcal{S}_{\to i,k} \subset \mathcal{N}_{\to i,k}$ of paired "virtual anchors" and update new weights according to the likelihood

$$w_{i,k}^{(p)} \propto p(\mathbf{z}_{i,k}|\boldsymbol{\theta}_{i,k}^{(p)}, \boldsymbol{\theta}_{\mathcal{S}\to i,k}^{(p)}) = p(\mathbf{z}_{i,k}|\boldsymbol{\theta}_{i\cup\mathcal{S},k}^{(p)}), p = 1, \ldots, P,$$

normalize them to sum to unity, and compute the approximate Minimum Mean Square Error (MMSE) estimator as the second filter/fusion output $\hat{\boldsymbol{\theta}}_{i,k} \approx \sum_{p=1}^{P} w_{i,k}^{(p)} \boldsymbol{\theta}_{i,k}^{(p)}$.

4: **Regularized Resampling, Message Approximation, and Broadcast**

Thus, an approximate distribution called the sequential proposal density $\boldsymbol{\pi}(\boldsymbol{\theta}_{i,k}, \boldsymbol{\theta}_{\mathcal{S}\to i,k}|\boldsymbol{\theta}_{i,k-1}^{(p)}, \boldsymbol{\theta}_{\mathcal{S}\to i,k^-}^{(p)}, \mathbf{z}_{i,1:k})$ is used instead, from which one can easily draw samples. One popular embodiment thus consists in using the mobility model as the sequential proposal density [2], [11], [13] i.e., $\boldsymbol{\pi}(\cdot) = p(\boldsymbol{\theta}_{i,k}|\boldsymbol{\theta}_{i,k-1}^{(p)}) \prod_{j\in\mathcal{S}_{i,k}} p(\boldsymbol{\theta}_{j,k_i}|\boldsymbol{\theta}_{j,k}^{(p)})$.

This PF is called bootstrap PF. To the best of our knowledge, most of PFs are practically implemented in a bootstrap manner due to its simplicity. We then propose to apply this popular bootstrap PF as the core filter/fusion engine of our CLoc framework, as described in Algorithm 1 (incl. also side CAM reception, message approximation and CAM broadcast steps).

## III. Proposed Performance-Enhancing Technique

### A. Bootstrap PF: Problem Formulation

As aforementioned, in bootstrap PF we use the mobility model as the sequential proposal density, which does not account for the most recent observation. Hence, particles are generated from the mobility model (Algorithm 1, Step 2), whereas the corresponding weights are updated by simply computing the measurement likelihood given the current observation and the states of these predicted particles (Algorithm 1, Step 3). This suboptimal choice, unfortunately, can lead to specific problems under some circumstances.

Fist, the efficiency of the bootstrap PF relies critically on the "match" between between these two densities [11], [12]. Since the mobility model is not conditioned on the observation on which likelihood relies, there might exist a "mismatch" between them. For instance, if the ranging technology is highly accurate leading to concentrated (joint) likelihood but the mobility is not (due to either imperfect prediction model or poor initialization[6]), then only a few particles close to the true state are assigned significant weights, resulting in particles

[6]In general, it is reasonable to assume rather poor initial guess. For example, in order to perform IR-UWB V2V ranges, vehicles need to be paired. During this period, they can only rely on GNSS, which does not always provide accurate location beliefs.

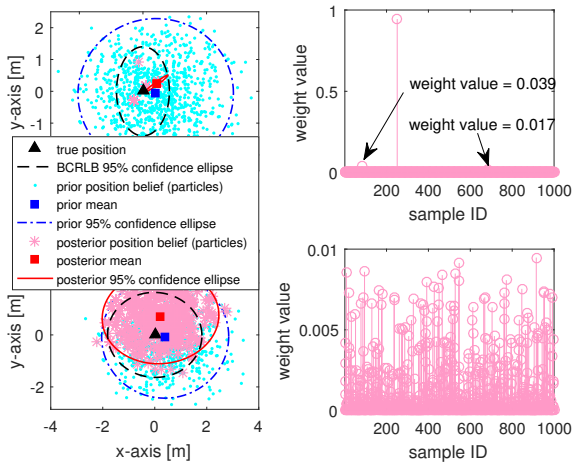


Fig. 2. Illustration of particle depletion when fusing accurate IR-UWB ranges with GNSS (top subfigures) and no depletion when using inaccurate RSSIs (bottom subfigures) in a bootstrap PF. The scenario is a 9-node VANETs and the "ego" vehicle is vehicle 5 as shown in Fig. 4 in one snapshot. Left top/bottom subfigures illustrate the position estimate and the corresponding confidence ellipse at "ego" car, when fusing 8 IR-UWB ranges/RSSIs w.r.t. other cars with "ego" and neighboring prior beliefs in comparison with theoretical performance bounds. Right top/bottom subfigures show the updated weights accounting for the collapsed/distributed particle cloud approximating the "ego" posterior density. Main simulation parameters include: prior bias $\sim \mathcal{U}(0, 0.5)$ [m], prior 1-$\sigma$ uncertainty of 1 [m] on both $x$- and $y$-axes independently, $\sigma_{\text{UWB}} = 0.2$ [m], $\sigma_{\text{Sh}} = 2.5$ [dB], and 1000 particles.

depletion. As a result, the posterior density support is concentrated to a submanifold of the state space, leading possibly to be overconfident in biased location estimates. Fig. 2 illustrates this phenomenon with a single snapshot simulation. If, on the one hand, the neighbors' positions are perfectly known, which may not be reasonable in a pure VANET case, the "ego" posterior density is concentrated but located close to the true position. However such estimation is unstable since it does not fix the particle depletion. If, on the other hand, the neighbors' positions are biased (either strongly or weakly), these terms are propagated to the "ego" position estimate, which thus quickly converges to an inaccurate value, whereas extremely high confidence is still given to the result (See Fig. 2 (left top)). Such a situation can be fatal: this malicious information is then broadcast over the network and degrades the position accuracy of all neighbors. Note that the particle depletion does not occur when fusing inaccurate RSSIs because their (joint) likelihood is a broad density indicating that most particles retain a meaningful weight (Fig. 2 (bottom)).

Second, though the bootstrap PF is implemented in a distributed manner, in the VANET context, the state must be augmented to account for the uncertainties of the "virtual anchors" i.e., neighboring beliefs (See Algorithm 1, Step 2 and 3). Put differently, the position estimation is performed in high-dimensional space. In this case, there might be no particle in the vicinity to the correct augmented state because the number of particles cannot be sufficiently high to cover all relevant regions concerned by the concentrated (joint) likelihood density [12].

Hence, jointly or separately, the compact uncertainty of the measurements (e.g., accurate IR-UWB ranges) and the high

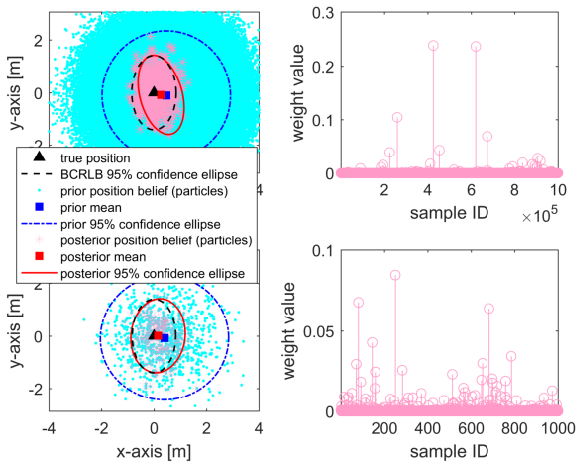


Fig. 3. Illustration of 2 solutions for particle depletion when fusing accurate IR-UWB ranges with GNSS positions in a bootstrap PF. The two left subfigures illustrate the position estimates and the corresponding confidence ellipses in comparison with theoretical bounds when using a conventional approach with $10^6$ particles (top) or the proposed adaptive dithering technique with 1000 particles only (bottom). Right top and bottom subfigures show the updated weights yielding meaningful particle clouds. Except the number of particles and the adaptive dithering technique, the considered scenario and simulation parameters are the same as that in Fig. 2.

dimensionality of the state space both lead to the inefficiency of the bootstrap PF in the very fusion context.

### B. BCRLB-based Adaptive Dithering

To avoid particle depletion, we aim at having more particles with significant assigned weights in order to maintain particles diversity and therefore, to avoid overconfidence issues. One immediate and intuitive approach is to increase the number of particles. Such a solution can solve the problem at the expense of extremely high computation load, as shown in Fig. 3 (top). However, it is unsuitable to real-time vehicular tracking under high mobility.

Another simple but efficient solution called dithering is to use a smoothed (joint) likelihood i.e., to assume deliberately more noise in the observation model than the actual noise affecting real measurements [11], [12]. Nevertheless, if performed systematically, accurate measurement information is partly lost and the extent to which noise must be increased in the observation model is questionable. Moreover, as the (joint) likelihood depends on the number of cooperative "virtual anchors", the more numerous the cooperative neighbors, the sharper the (joint) likelihood. Said differently, an excessively smoothed (joint) likelihood in case of a few neighbors tends to loose information whereas a too slightly smoothed likelihood with a high number of neighbors does not solve the depletion problem. Thus, we propose a novel adaptive dithering technique to solve the problem. The idea is to predict the actual performance of the IR-UWB range-based fusion based on positioning Bayesian Cramér-Rao Lower Bound (BCRLB), which in first approximation can capture both "ego" and anchors' uncertainties [3] in a dynamic tracking context. Thus far, we can rely on this performance bound to adjust the minimum required amount of added noise in the perception model

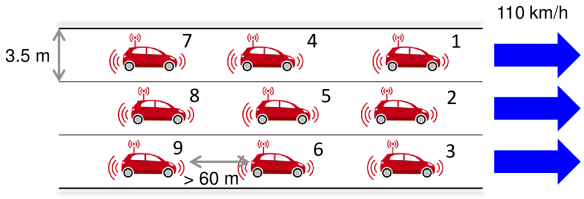


Fig. 4. Evaluated VANET and related attributes in highway scenario.

by manipulating the assumed ranging standard deviation (SD). In this paper, adaptive dithering is implemented in an iterative approach, where we start with an *a priori* nominal ranging SD (i.e., corresponding to the best expected technology potential). In every iteration, we gradually increase this SD until the posterior density becomes meaningful and reliable i.e., its empirical covariance is no more smaller than the predicted BCRLB, avoiding overconfidence without spoiling too much the benefits from high-accuracy IR-UWB range measurements.

The BCRLB for IR-UWB range-based CLoc is calculated as follows. At "ego" time $t_{i,k}$ before the fusion, $\mathbf{x}_{i,k} \sim p(\mathbf{x}_{i,k}|\mathbf{z}_{i,1:k-1})$, the position of the "ego" $i$ and $\mathbf{x}_{j,k_i} \sim p(\mathbf{x}_{j,k_i}|\mathbf{z}_{j,1:k})$, $j \in \mathcal{S}_{\to i,k}$, the positions of its "virtual anchors", the Bayesian Fisher Information Matrix (FIM) is [3]

$$\mathbf{J}^B_{i,k} = \mathbf{J}^P_{i,k} + \sum_{j \in \mathcal{S}_{\to i,k}} [(\mathbf{J}^P_{j,k_i})^{-1} + (\mathbf{J}^M_{j\to i,k})^{-1}]^{-1}, \quad (5)$$

where $\mathbf{J}^P_{i,k}$, $\mathbf{J}^P_{j,k_i}$ are the *a priori* FIMs of the positions of the "ego" $i$ and its "virtual anchors" $j \in \mathcal{S}_{\to i,k}$ respectively, while $\mathbf{J}^M_{j\to i,k}$ denotes the FIM obtained from the link measurement $(j \to i)$. In particular, the prior FIMs are defined as

$$\mathbf{J}^P_{i,k} = \mathbb{E}_{\mathbf{x}_{i,k}} \left\{ -\Delta^{\mathbf{x}_{i,k}}_{\mathbf{x}_{i,k}} \log p\left(\mathbf{x}_{i,k}|\mathbf{z}_{i,1:k-1}\right) \right\}, \quad (6a)$$

$$\mathbf{J}^P_{j,k_i} = \mathbb{E}_{\mathbf{x}_{j,k_i}} \left\{ -\Delta^{\mathbf{x}_{j,k_i}}_{\mathbf{x}_{j,k_i}} \log p\left(\mathbf{x}_{j,k_i}|\mathbf{z}_{j,1:k}\right) \right\}. \quad (6b)$$

Assuming $p(\mathbf{x}_{i,k}|\mathbf{z}_{i,1:k-1})$ and $p(\mathbf{x}_{j,k_i}|\mathbf{z}_{j,1:k})$, $j \in \mathcal{S}_{\to i,k}$ are Gaussian with covariance matrices $\mathbf{\Sigma}_{j,k|k-1}$ and $\mathbf{\Sigma}_{j,k_i|k}$ respectively in first approximation, thus $\mathbf{J}^P_{i,k} = \mathbf{\Sigma}^{-1}_{j,k|k-1}$ and $\mathbf{J}^P_{j,k_i} = \mathbf{\Sigma}^{-1}_{j,k_i|k}$. On the other hand, the term related to the measurements is calculated using Monte Carlo approach as

$$\begin{aligned}
\mathbf{J}^M_{j\to i,k} &= \mathbb{E}_{z_{j\to i,k},\mathbf{x}_{i,k},\mathbf{x}_{j,k_i}} \left\{ -\Delta^{\mathbf{x}_{i,k}}_{\mathbf{x}_{i,k}} \log p\left(z_{j\to i,k}|\mathbf{x}_{i,k},\mathbf{x}_{j,k_i}\right) \right\} \\
&= \frac{1}{\sigma^2_{\text{UWB}}} \mathbb{E}_{\mathbf{x}_{i,k},\mathbf{x}_{j,k_i}} \left\{ \frac{(\mathbf{x}_{i,k} - \mathbf{x}_{j,k_i})(\mathbf{x}_{i,k} - \mathbf{x}_{j,k_i})^\dagger}{\|\mathbf{x}_{i,k} - \mathbf{x}_{j,k_i}\|^2} \right\} \\
&\approx \frac{1}{\sigma^2_{\text{UWB}}} \frac{1}{P} \sum_{p=1}^{P} \frac{(\mathbf{x}^{(p)}_{i,k} - \mathbf{x}^{(p)}_{j,k_i})(\mathbf{x}^{(p)}_{i,k} - \mathbf{x}^{(p)}_{j,k_i})^\dagger}{\|\mathbf{x}^{(p)}_{i,k} - \mathbf{x}^{(p)}_{j,k_i}\|^2}.
\end{aligned}$$

The overall adaptive dithering technique is summarized in Algorithm 2 and should be triggered before Step 3 in Algorithm 1. Note that $\{d_1, d_2\}$ in line 10 of Algorithm 2 are tuning parameters indicating how close the estimation approaches the theoretical performance bound and can be set to small arbitrary values between $[0, 0.5]$.

## IV. Performance Evaluation

### A. Simulation Settings and Scenarios

In our MATLAB-based evaluations, we model a common 3-lane highway, where 9 ITS-G5 connected vehicles endowed

**Algorithm 2** BCRLB-based Dithering (iteration $k$, "ego" car $i$)

Compute the Bayesian FIM $\mathbf{J}_{i,k}^{B}$ for IR-UWB-based CLoc
Compute the principal components $\{\lambda_{(1)}, \lambda_{(2)}\}$ by finding the eigenvalues of $[\mathbf{J}_{i,k}^{B}]^{-1}$, $\lambda_{(1)} \leq \lambda_{(2)}$
Begin with the actual ranging SD $\tilde{\sigma}_{\text{UWB}} = \sigma_{\text{UWB}}$
**do**
    Update the weights $\tilde{w}_{i,k}^{(p)} \propto p\left(\mathbf{z}_{\mathcal{S}\to i,k} \middle| \mathbf{x}_{i,k}^{(p)}, \mathbf{x}_{\mathcal{S}\to i,k}^{(p)}, \tilde{\sigma}_{\text{UWB}}\right)$
    Normalize the weights to sum to unity
    Compute the mean $\mathbb{E}\left\{\mathbf{x}_{i,k} | \mathbf{z}_{\mathcal{S}\to i,k}, \tilde{\sigma}_{\text{UWB}}\right\} = \sum_{p=1}^{P} \tilde{w}_{i,k}^{(p)} \mathbf{x}_{i,k}^{(p)}$
    Compute empirical covariance $\text{cov}\left(\mathbf{x}_{i,k} \middle| \mathbf{z}_{\mathcal{S}\to i,k}, \tilde{\sigma}_{\text{UWB}}\right) = \sum_{p=1}^{P} \tilde{w}_{i,k}^{(p)} \left(\mathbf{x}_{i,k}^{(p)} - \mathbb{E}\{\mathbf{x}_{i,k}|\cdot\}\right) \left(\mathbf{x}_{i,k}^{(p)} - \mathbb{E}\{\mathbf{x}_{i,k}|\cdot\}\right)^{\dagger}$
    Compute the principal components $\{\lambda'_{(1)}, \lambda'_{(2)}\}$ by finding the eigenvalues of $\text{cov}\left(\mathbf{x}_{i,k} \middle| \mathbf{z}_{\mathcal{S}\to i,k}, \tilde{\sigma}_{\text{UWB}}\right)$, $\lambda'_{(1)} \leq \lambda'_{(2)}$
    Add dither noise $\Delta$ to perception model $\tilde{\sigma}_{\text{UWB}} = \tilde{\sigma}_{\text{UWB}} + \Delta$
**while** $\sqrt{\lambda'_{(1)}} \leq (1+d_1)\sqrt{\lambda_{(1)}}$ **or** $\sqrt{\lambda'_{(2)}} \leq (1+d_2)\sqrt{\lambda_{(2)}}$
**return** $\tilde{\sigma}_{\text{UWB}}$

TABLE I
MAIN SIMULATION PARAMETERS

| Parameter | Value |
|---|---|
| Memory level $\alpha$ | 0.95 |
| Tangential acc. uncertainty | 1 [m/s$^2$] |
| Perpendicular acc. uncertainty | 0.1 [m/s$^2$] (to satisfy road constraints) |
| Sampling period $\Delta T$ | 0.1 [s] |
| SD of GNSS errors in $x$- and $y$-axes | 1.5 [m] (SBAS like EGNOS[a]) [14] |
| GNSS refresh rate | 10 [Hz] |
| CAM rate | 10 [Hz] (critical) |
| IR-UWB ranging rate | 5 [Hz] (hypothesis) |
| SD of IR-UWB ranging noise | 0.2 [m] |
| Path loss exponent $n_p$ | 1.9 (V2V in highways) [10] |
| SD of shadowing $\sigma_{\text{Sh}}$ | 2.5 [dB] (V2V in highways) [10] |
| Number of particles | 1000 |
| Initial positional error in $x$- and $y$-axes | 1 [m] (RMS) (plausible hypothesis) |
| Initial velocity errors in $x$- and $y$-axes | 0.1 [m] (RMS) (plausible hypothesis) |

[a] Satellite-Based Augmentation System (SBAS) and its variant European Geostationary Navigation Overlay Service (EGNOS).

with IR-UWB ranging capabilities are driving steadily in a common direction at the average speed of 110 km/h (i.e., about 30 m/s) for 60 seconds, as shown in Fig. 4. The main simulation parameters are summarized in Table I.

In our comparative study, we consider three different localization configurations, namely the filtered standalone GNSS (non-CLoc scheme), the fused GNSS+RSSI, and the GNSS+IR-UWB. In the GNSS+IR-UWB scheme, we compare the localization performance of bootstrap PF with and without adaptive dithering. We also benchmark our proposal with the well-known Extended Kalman Filter (EKF) to verify that the solved problem is not uniquely PF-dependent.

### *B. Results*

The results are summarized in Fig. 5 by means of empirical Cumulative Distribution Functions (CDFs) and in Fig. 6 in terms of the perceived 1-$\sigma$ estimation error in the filter, accounting for the (over-)confidence in estimated values. It is seen that the fused GNSS+RSSI option only slightly outperforms the standalone GNSS in terms of accuracy. This observation is not contradictory with previous studies [2], [3], [6], which claim more substantial benefits from RSSI. We indeed use herein a much more advanced GNSS technology (i.e., EGNOS) whereas these studies consider only the Standard Positioning Service (SPS). Thus, the standalone filtered GNSS (EGNOS) achieves rather high accuracy already,

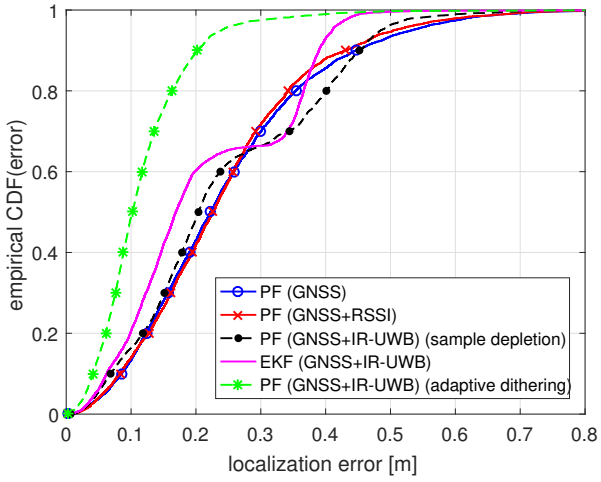


Fig. 5. Empirical CDF of localization errors for different fusion techniques, schemes, and measurements/technologies.

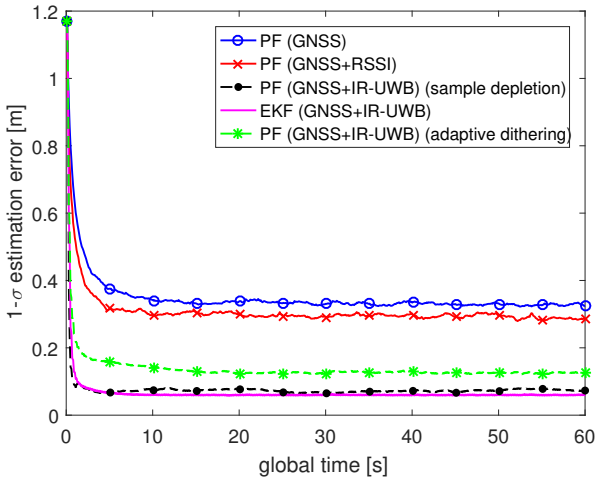


Fig. 6. Average 1-$\sigma$ estimation errors perceived by fusion filters for different fusion techniques, schemes, and measurements/technologies.

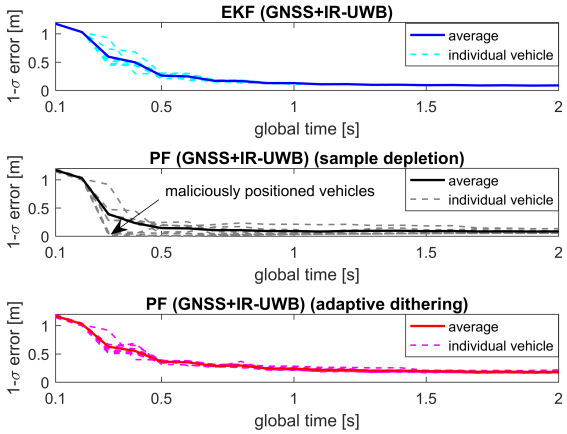


Fig. 7. 1-$\sigma$ estimation errors perceived by fusion filters for each vehicle during the first 2 seconds for the fused GNSS+IR-UWB ranges using EKF (top), conventional PF (middle), and PF with adaptive dithering (bottom).

making RSSI-based fusion schemed more questionable since RSSI radiolocation metrics are neither accurate enough (in comparison with GNSS) nor sufficiently reliable in terms of their ranging interpretation.

Fig. 5 also shows that the fused GNSS+IR-UWB scheme, relying on the bootstrap PF (without dithering) or the EKF indifferently, yields "local" gains in comparison with the GNSS (set as a reference). For example, their performances are superior in terms of the median error (CDF of 50%) and in high error regimes (e.g., CDF of 95%) but degraded in the low error regime below 0.35 m. This multimodal CDF shape indicates that some vehicles (i.e., a sub-group of the whole fleet) are rather poorly positioned when using these algorithmic schemes. For bootstrap PF, this mostly comes from particle depletion, leading to over-convergence issues i.e., the estimates rapidly converge to inaccurate estimates but extremely high confidence is given to these inaccurate values. Comparing Fig. 5 and Fig. 6 confirms this observation (actual 1-$\sigma$ localization error of 0.32 m (CDF of 68%) vs. perceived 1-$\sigma$ estimation error of 0.079 m). Regarding the EKF, this is due to the poor but realistic initialization (See Table I). It is worth reminding that the goodness of the linearization in EKF depends on the state uncertainty besides the nonlinear models [12]. Note that when EKFs converge to inaccurate values, they also become somehow overconfident (actual 1-$\sigma$ localization error (CDF of 68%) of 0.33 m vs. perceived 1-$\sigma$ estimation error of 0.062 m provided by Fig. 5 and Fig. 6 respectively). A closer look in Fig. 5 reveals that the EKF surprisingly outperforms the conventional bootstrap PF. Though Fig. 6 shows that the fused GNSS+IR-UWB using bootstrap PF and EKF have comparative average perceived 1-$\sigma$ estimation errors once convergence is achieved, Fig. 7 (top and middle) focus on the same metric at individual vehicles (along with the average over the entire fleet). It is seen in Fig. 7 (middle) that extremely severe particle depletion occurs at several vehicles leading to malicious "virtual anchors" harmful to CLoc at other vehicles (i.e., perceived 1-$\sigma$ estimation error is almost null so that the vehicles are perceived as true reliable anchors but their estimated positions are actually biased).

As expected, the bootstrap PF with adaptive dithering for GNSS+IR-UWB fusion provides the best accuracy as shown in Fig. 5. Specifically, we observe significant relative drops of 54%, 55%, 50%, and 40% in median errors and 42%, 39%, 42%, and 33% in worst-case errors (e.g., CDF of 90%) in comparison with the classical bootstrap PFs (GNSS, GNSS+RSSI, GNSS+IR-UWB), and EKF (GNSS+IR-UWB) respectively. In addition, since the particle depletion is completely solved by adaptive dithering, the overconfidence problem disappears and one can thus draw maximum benefits from accurate IR-UWB range measurements (actual 1-$\sigma$ localization error of 0.13 m vs. perceived 1-$\sigma$ estimation error of 0.15 m indicated by Fig. 5 and Fig. 6 respectively).

## V. Conclusion and Future Work

Motivated by the need to remove estimation biases propagation and overconfidence in classical PF-based CLoc when fusing GNSS position and IR-UWB ranges to imperfect positioned neighbors, we have proposed an adaptive dithering technique based on a BCRLB criterion to maximize benefits from accurate IR-UWB technology and PF in nonlinear fusion. By applying the proposed solution to the classical PF-based CLoc, we found that: (i) there is no need to use a huge number of particles to avoid particles depletion in high-dimensional estimation with concentrated (joint) measurement likelihood; (ii) aforementioned harmful effects caused by particles depletion are effectively mitigated by an adequate amount of dither noise based on BCRLB, hence, minimizing the performance degradation caused by information loss. Future work would investigate how to reduce the number of iterations of the proposed iterative technique by monitoring the alternation of dither noise w.r.t. dynamic number of "virtual anchors", thus, a fast differential variant can be developed.

## Acknowledgment

This work has been performed in the frame of the *HIGHTS* project, which is funded by the European Commission (636537-H2020).

EURECOM acknowledges the support of its industrial members, namely, BMW Group, IABG, Monaco Telecom, Orange, SAP, ST Microelectronics, and Symantec.

## References

[1] R. Parker and S. Valaee, "Vehicular node localization using received-signal-strength indicator," *IEEE Trans. on Veh. Technol.*, vol. 56, pp. 3371–3380, Nov. 2007.

[2] G. M. Hoang, B. Denis, J. Härri, and D. T. M. Slock, "Breaking the gridlock of spatial correlations in GPS-aided IEEE 802.11p-based cooperative positioning," *IEEE Trans. on Veh. Technol.*, vol. PP, Jun. 2016.

[3] G. M. Hoang, B. Denis, J. Härri, and D. T. M. Slock, "Select thy neighbors: Low complexity link selection for high precision cooperative vehicular localization," in *Proc. VNC'15*, pp. 36–43, Dec. 2015.

[4] J. Yao, A. Balaei, M. Hassan, N. Alam, and A. Dempster, "Improving cooperative positioning for vehicular networks," *IEEE Trans. on Veh. Technol.*, vol. 60, pp. 2810–2823, Jul. 2011.

[5] G. M. Hoang, B. Denis, J. Härri, and D. T. M. Slock, "Cooperative localization in GNSS-aided VANETs with accurate IR-UWB range measurements," in *Proc. WPNC'16*, Oct. 2016.

[6] G. M. Hoang, B. Denis, J. Härri, and D. T. M. Slock, "Distributed link selection and data fusion for cooperative positioning in GPS-aided IEEE 802.11p VANETs," in *Proc. WPNC'15*, pp. 1–6, Mar. 2015.

[7] N. Drawil and O. Basir, "Intervehicle-communication-assisted localization," *IEEE Trans. on Intel. Transp. Syst.*, vol. 11, pp. 678–691, Sept. 2010.

[8] "Intelligent Transport Systems (ITS); Vehicular Communications; Basic Set of Applications; Part 2: Specification of Cooperative Awareness Basic Service," *ETSI Std. EN 302 637-2 V1.3.2*, Oct. 2014.

[9] M. Maman, B. Denis, M. Pezzin, B. Piaget, and L. Ouvry, "Synergetic MAC and higher layers functionalities for UWB LDR-LT wireless networks," in *Proc. ICUWB'08*, vol. 3, pp. 101–104, Sept. 2008.

[10] L. Cheng, B. E. Henty, F. Bai, and D. D. Stancil, "Highway and rural propagation channel modeling for vehicle-to-vehicle communications at 5.9 GHz," in *Proc. AP-S'08*, pp. 1–4, Jul. 2008.

[11] M. Arulampalam, S. Maskell, N. Gordon, and T. Clapp, "A tutorial on particle filters for online nonlinear/non-Gaussian Bayesian tracking," *IEEE Trans. on Sig. Proc.*, vol. 50, pp. 174–188, Feb. 2002.

[12] S. Thrun, W. Burgard, and D. Fox, *Probabilistic Robotics (Intelligent Robotics and Autonomous Agents)*. The MIT Press, 2005.

[13] S. Särkkä, *Bayesian Filtering and Smoothing*. New York, NY, USA: Cambridge University Press, 2013.

[14] DoD, "GPS Standard Positioning Service (SPS) performance standard," Sep. 2008.